Acousto-optic laser projection systems for displaying TV information

2015 Quantum Electron. 45 283

(http://iopscience.iop.org/1063-7818/45/4/283)

Quantum Electronics **45** (4) 283–300 (2015)

REVIEW

PACS numbers: 42.79.Jq; 43.35.Sx; 42.55.Lt
DOI: 10.1070/QE2015v045n04ABEH015421

Acousto-optic laser projection systems for displaying TV information

Yu.V. Gulyaev, M.A. Kazaryan, Yu.M. Mokrushin, O.V. Shakin

Abstract. **This review addresses various approaches to television projection imaging on large screens using lasers. Results are presented of theoretical and experimental studies of an acousto-optic projection system operating on the principle of projecting an image of an entire amplitude-modulated television line in a single laser pulse. We consider characteristic features of image formation in such a system and the requirements for its individual components. Particular attention is paid to nonlinear distortions of the image signal, which show up most severely at low modulation signal frequencies. We discuss the feasibility of improving the process efficiency and image quality using acousto-optic modulators and pulsed lasers. Real-time projectors with pulsed line imaging can be used for controlling high-intensity laser radiation.**

Keywords: *acousto-optic modulators and deflectors, acousto-optic interaction, pulsed solid-state lasers, metal vapour lasers, paratellurite crystal.*

1. Introduction

Devices capable of displaying a large amount of information with high image quality are of practical interest for scientific and technological applications, such as optical information processing, information storage in various media, displaying television images and communications, where large information flows have to be dealt with in real time.

The world's leading electronics companies have focused great effort on designing television information display systems using laser sources. Lasers ensure high brightness in combination with colour contrast unattainable for lamps and phosphors. Pulsed lasers stand out among laser sources because they enable efficient nonlinear conversion of light to other parts of the visible range, thus covering the entire spectral region our eyes are sensitive to. One attractive approach to real-time imaging with such lasers is pulsed projection of an image of an amplitude-modulated ultrasonic line, which fills the aperture of an acousto-optic modulator.

The modulation technique under consideration needs no high-speed line scanning and, in contrast to other existing techniques that employ modulator arrays, there is no discrete image structure. An image is created in real time, with no delay, and is better suited to sequential information transfer through a communications channel. The dimensions of the image can readily be varied, without changing the modulation device. In the case of information storage in various media, coherent optical information processing is possible. The possibility of using all-acousto-optic control devices in the system under consideration allows one in a diversity of applications to do without mechanical control devices, such as mirror scanners, rotating multifaceted prisms and two-dimensional and linear micromirror arrays. Moreover, the crystalline media of the modulators in this system can withstand high average and peak laser output powers, which allows the systems under consideration to be used in technological applications.

Even though the pulsed imaging approach has been known for a long time, there are many unresolved issues pertaining to the effectiveness and quality of imaging with the now most efficient acousto-optic modulators (AOMs), based on paratellurite (TeO_2) crystals, using amplitude-modulated ultrasound. The difficulty lies in that acousto-optic diffraction should be considered for an anisotropic gyrotropic medium, such as a TeO_2 crystal, and an intermediate mode of diffraction of light from sound. It is also necessary to assess the feasibility of practical application of this approach for displaying full-colour television information on large screens in a high-definition standard.

At present, the greatest potential for pulsed imaging is offered by metal vapour lasers, including the copper vapour laser, and frequency-doubled neodymium lasers. An important issue is the ability to optimise appropriate laser output parameters.

2. Development of laser television information display systems

One of the first studies concerned with a television information display system using a laser was reported by Korpel et al. [1]. As a light beam, they employed cw He–Ne laser radiation. The modulator used was an ultrasonic water cell, in which an acoustic wave was excited at a frequency f = 41.5 MHz. The motion of the line on the screen was stopped by an acousto-optic deflector (AOD) using water as the

Yu.V. Gulyaev V.A. Kotel'nikov Institute of Radio Engineering and Electronics, Russian Academy of Sciences, Mokhovaya ul. 11/7, 125009 Moscow, Russia; e-mail: gulyaev@cplire.ru;
M.A. Kazaryan P.N. Lebedev Physics Institute, Russian Academy of Sciences, Leninsky prosp. 53, 119991 Moscow, Russia; e-mail: kazarmishik@yahoo.com;
Yu.M. Mokrushin JSC D.V. Efremov Institute of Electrophysical Apparatus, Doroga na Metallostroi 3, pos. Metallostroi, 196641 St. Petersburg, Russia; e-mail: yrmok@yandex.ru;
O.V. Shakin Ioffe Physical Technical Institute, Russian Academy of Sciences, Politekhnicheskaya ul. 26, 194021 St. Petersburg, Russia

Received 27 February 2014; revision received 16 May 2014
Kvantovaya Elektronika **45** (4) 283–300 (2015)
Translated by O.M. Tsarev

acousto-optic medium, which deflected an incident modulated light beam in the direction opposite to that of picture motion on the screen. Vertical scanning was ensured by an electromagnetic mirror galvanometer. At a video channel bandwidth of 3.15 MHz, the system made it possible to obtain 200 resolution elements per line. Because of the high acoustic attenuation (1.5 dB cm^{-1} at f = 30 MHz), the water-cell AOMS used in the first experiments operated at rather low ultrasound frequencies, which made it impossible to obtain a wide modulation frequency band of the video channel. Moreover, at high ultrasonic signal power levels such cells had a relatively short service life.

The first television systems with laser beam scanning employed cw inert-gas [argon (λ = 476.5, 514.5 and 488.0 nm) and krypton (λ = 647.1 nm)] lasers, which generated just a few watts of single-mode output radiation. These systems reached their peak development in the 1970s–1980s [2]. In such devices, the argon or krypton laser output intensity is modulated by an acousto-optic [3, 4] or electro-optical [5–8] modulator and sequential horizontal and vertical scanning is ensured by AODs [4, 7–10] or optomechanical scan systems, such as rotating polygon mirrors [5, 11, 12], multifaceted prisms [7], galvanometers [7, 12] and bimorph elements [6].

The main parameters characterising the operation of an information display system with continuous light beam scanning include the number of resolvable elements per line (which is determined by the product of the modulation frequency bandwidth in the video channel and the television line time) and the number of resolvable lines per frame. These parameters are determined by the characteristics of the spatial modulators and deflectors of light in the system. The choice of light beam modulation and deflection methods depends on the requirements for a particular information display or storage system. At low modulation frequencies ($\leqslant$10 MHz), AOMs are superior in performance to electro-optical modulators (EOMs) [13]. The latter are preferable at higher modulation frequencies. AOMs allow one to obtain larger contrast ratios at low frequencies in comparison with EOMs.

Optomechanical deflectors were used when colour images with low light loss and high resolution in lines and frames were needed. Since such systems are dispersion-free, there is no problem of colour correction on the screen. Their drawbacks are the slow speed, difficult-to-achieve necessary light beam deflection accuracy and stability and the sensitivity to mechanical vibrations. To eliminate these drawbacks, use was made of complex self-tuning systems and high-speed synchronous motors with magnetic and gas-dynamic supports [12]. AODs were successfully used in less expensive systems for obtaining monochrome images [7]. They have attracted considerable attention because they offer a simple beam steering algorithm, have small dimensions and contain no moving parts.

The highest achievement in designing cw laser television information display systems was a colour display developed by the Japanese companies NHK and Hitachi for enhanced-definition television [2, 12]. It displayed 1125 lines along the image height and had a video signal passband of up to 30 MHz. At a 6 W sum power of the laser sources (4 W from the argon laser and 2 W from the krypton laser), the system offered the possibility of high-quality imaging on a 3-m^2 screen. At a screen gain of 4, the image brightness was 37.6 cd m^{-2}. Despite the high image quality, such systems have not found wide application because of the low efficiency (0.05%) of the laser sources used.

One of the weakest links of the mechanical television image scanning system with cw light sources is the rapidly rotating polygon mirror, which produces television lines. The rotational speed of the polygons reaches 30–60 krpm. The fabrication quality of these devices should meet very stringent requirements.

Serious difficulties in producing a uniform horizontal television line are also encountered when acousto-optic deflectors of a cw laser beam are used [2].

To avoid high-speed scanning, a pulsed laser-based acousto-optic television projection display system was proposed in 1974 [14]. It was an upgraded version of the television system developed in 1938–1939 at Scophony Ltd (UK) [15, 16], in which a high-power mercury lamp was used as a light source, and an ultrasonic liquid cell served as a modulator. The optical scheme of this device is presented in Fig. 1.

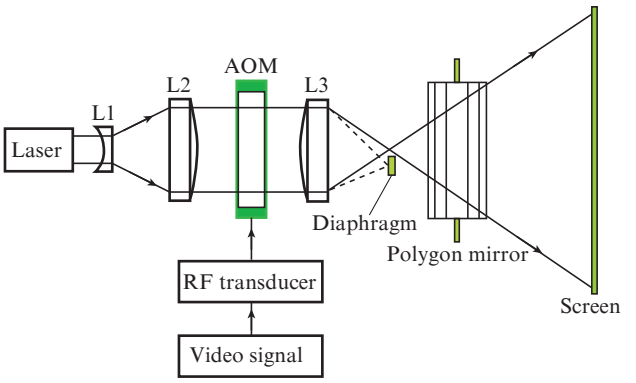

Figure 1. Schematic of the acousto-optic pulsed laser television system.

The laser pulse repetition rate should be equal to the horizontal scan rate and the cell length should be

$$L = T_{str} v, \tag{1}$$

where T_{str} is the television line time and v is the speed of sound in the AOM material.

After diffracting from an ultrasonic wave and passing through an optical projection system, each laser pulse imaged a line on the screen. To obtain a sharp image, the laser pulse duration should be shorter than or equal to the time needed for one resolvable image element to pass through the acousto-optic medium of the modulator. In such a system, the total number of resolvable elements per line is approximately given by

$$N_{str} \simeq \frac{T_{str}}{\tau + \tau_0} \simeq \frac{T_{str}\Delta f_0}{1 + \tau_0 \Delta f_0}, \tag{2}$$

where τ is the 'duration' of one resolvable element; τ_0 is the laser pulse duration; and Δf_0 is the modulation signal bandwidth.

It follows from (2) that, to obtain 300 resolvable elements per line at T_{str} = 60 μs and Δf_0 = 6 MHz, the pulse duration should be $\tau_0 \leqslant$ 30 ns. The laser pulse repetition rate should be equal to the horizontal frequency (15.625 kHz in

the SECAM system), with high average power and radiation directivity.

Yamamoto [14] proposed using a Q-switched Nd:YAG laser with a pulse repetition rate equal to the horizontal scan rate. Conversion to the visible range was planned to be performed via second harmonic generation in a lithium iodide nonlinear crystal. Vertical scanning in such a device was to be ensured by a polygon mirror. A candidate acousto-optic medium was an α crystal, with an ultrasound velocity of 2.44×10^5 cm s^{-1} and an ultrasound attenuation coefficient considerably smaller than that in water. At this ultrasound velocity, the crystal length for 'recording' an entire television line should be 15.5 cm. As pointed out by Yamamoto [14], using radiation of primary colours [blue (B), green (G) and red (R)] at wavelengths λ_B, λ_G and λ_R in appropriate power proportions one can make a television display system with one acousto-optic spatial light modulator. To this end, ultrasonic waves should be excited in the AOM at frequencies f_B, f_G and f_R that meet the condition

$$\lambda_B f_B = \lambda_G f_G = \lambda_R f_R = 2\sin\theta_B, \tag{3}$$

where θ_B is the angle of incidence of the light beam on the modulator, equal to the Bragg angle. The images at these wavelengths will then coincide. Yamamoto [14] made an attempt to build such a system, but because of the limited technical capabilities of the time (laser pulse parameters unsuited to the requirements for pulsed projection systems) and the lack of appropriate acousto-optic crystals the attempt was unsuccessful. In particular, the Nd:YAG laser generated pulses of 0.2 μs duration at a repetition rate of 300 Hz and the length of the acousto-optic cell was just one-tenth of the required one.

Further progress in pulsed television technology was ensured by the advent of repetitively pulsed high-power lasers emitting in the visible range: copper, gold and other metal vapour lasers and frequency-doubled Q-switched Nd:YAG lasers. In addition, advances in crystal growth enabled the preparation of high-performance acousto-optic crystals having low speeds of sound in certain crystallographic directions (TeO_2 and Hg_2Cl_2) and dimensions that enabled a standard television line ($T_{str} = 52$ μs) to be accommodated in the acoustic channel.

Good results in making a monochrome television system with a pulsed copper vapour laser were obtained in England [17] and Russia [18, 19]. Martinsen and Aylward [20] and Martinsen et al. [21] described a system operating on the same principle as in Refs [17, 19], in which a lamp-pumped frequency-doubled Q-switched pulsed Nd:YAG was used as the main laser. The average laser output power at $\lambda_G = 532$ nm was 16 W. The output of three such lasers was used to obtain the three primary colours for full-colour laser television imaging. The green colour was obtained using one laser ($\lambda_G = 532$ nm, $P_G = 16$ W). The red colour was provided by a dye laser pumped by the output of another frequency-doubled Nd:YAG laser ($\lambda_R = 615$ nm, $P_R = 15$ W). The blue colour was obtained using a frequency-doubled Ti:sapphire laser pumped by the third frequency-doubled Nd:YAG laser ($\lambda_B = 450$ nm, $P_B = 6$ W). The system operated in the NTSC standard and produced a colour television image on a screen 3.6×4.8 m in dimensions. The pulse duration of the lasers was 100 ns, which made it impossible to obtain high line resolution in the television projector. There was a report [22] on an increase in the average output power of blue light to 7 W ($\tau_0 = 80$ ns, pulse repetition rate $f_{rep} = 17$ kHz) at wavelengths from 430 to 460 nm in a Ti:sapphire laser with intracavity frequency doubling in a BiB_3O_6 (BBO) crystal, which was pumped by a frequency-doubled Q-switched neodymium laser.

A further breakthrough in the development of laser projection systems was made in the late 1990s to the early 2000s. This was associated with the advent of new, sufficiently powerful laser sources emitting in the green, blue and red spectral regions. All these sources relied on nonlinear conversion of IR radiation of solid-state or semiconductor lasers to the visible range. The most efficient conversion was achieved in pulsed mode using nonlinear optical single crystals or regular domain structure crystals [23–27].

In 1998, the German company Laser Display Technology (LDT) proposed new technology of laser projection systems for displaying television information [28–30], which was shortly thereafter commercialised by JENOPTIC Laser GmbH.

The laser source in such systems (Fig. 2) has a master oscillator–amplifier–nonlinear optical converter configuration. The master oscillator is a diode-pumped mode-locked Nd:YVO_4 laser operating at a wavelength $\lambda = 1064$ nm and generating 7-ps pulses with an average power of 4.5 W at a repetition rate of 80 MHz.

The pulses pass through four laser amplifier stages, with gain elements made of Nd:YVO_4 crystals, and their average power rises to 42 W. Next, the laser radiation is directed to the nonlinear optical conversion system, which comprises LiB_3O_5 (LBO) and $KTiOAsO_4$ (KTA) crystal doublers and sum frequency generators and a KTA optical parametric converter. The conversion system produces three laser beams at wavelengths of 532 ($P_G = 6.5$ W), 628 ($P_R = 7$ W) and 462 nm ($P_B = 4.8$ W). The beams are amplitude-modulated by an EOM or AOM. The three beams are then launched into one multimode optical fibre (where their powers are added together) and delivered to a horizontal/vertical scanning mirror system in the form of a polygon mirror (25 faces) and a vertical scanning electromagnetic galvanometer. An optical telescopic objective is used to form a television image on a projection screen. The overall modulated laser output power in the system under consideration is ~10 W. Because of the very short laser pulse durations (high electric field intensities of light waves), the IR to visible power conversion efficiency was 40%. In addition, because of the large bandwidth of the picosecond laser pulses, the image is free of speckles, which typically degrade the image quality in laser projectors. The maximum number of resolvable elements in an image in the system under consideration is determined by the ratio of the laser pulse repetition rate to the vertical frequency. At a frame rate of 25 Hz, after subtracting the flyback time this ratio is about 3×10^6. The output fibre end is common to all wavelengths, so there is no need to bring the colours into coincidence on the screen.

The system has drawbacks inherent in the high-speed mechanical mirror scanning system that was used previously in a scheme with cw gas-discharge lasers [2]. Moreover, it has a complex design because the laser cavities and nonlinear optical converters should be maintained at constant temperature.

Considerable effort is currently aimed at increasing the output power of the RGB lasers and simplifying their design

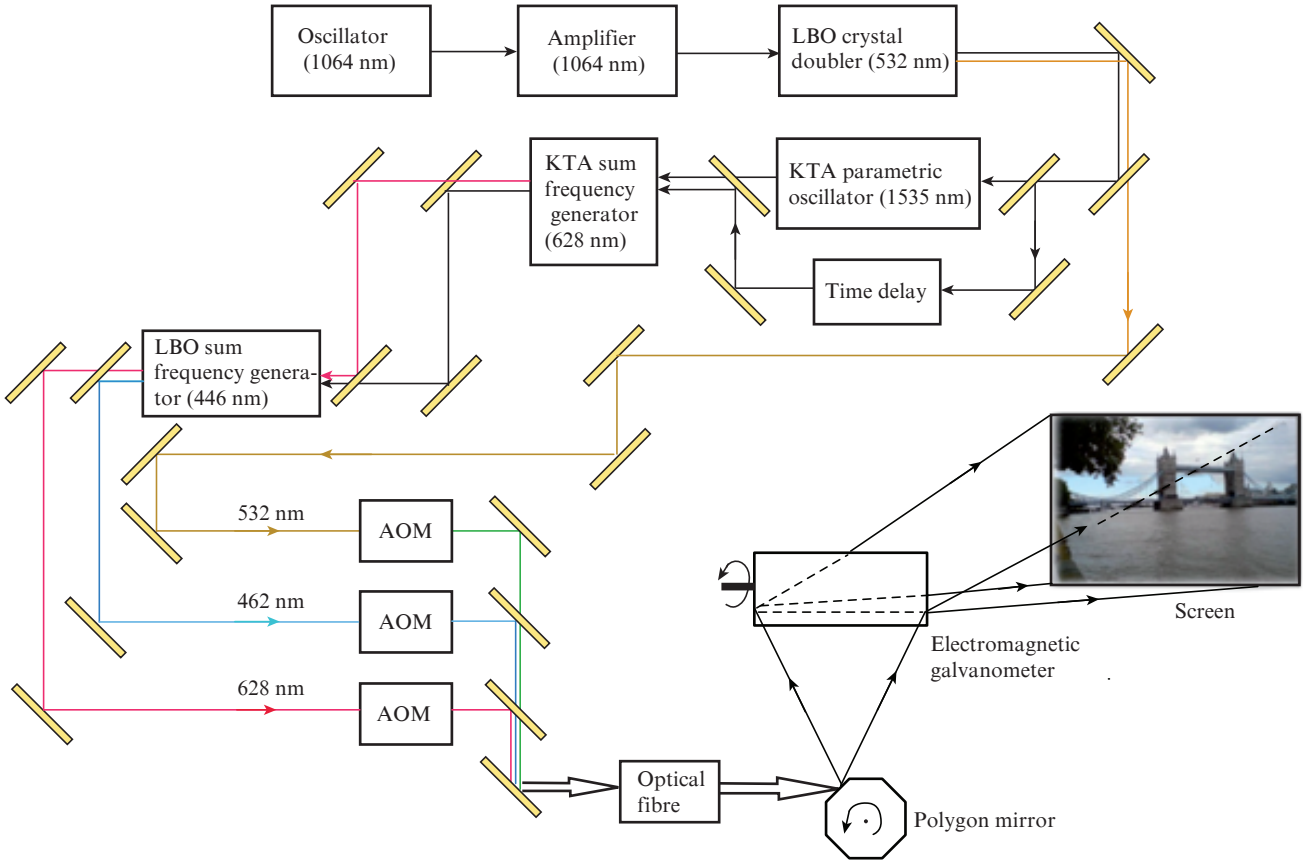

Figure 2. Block diagram of the LDT laser projector.

for the above projection system. Brunner et al. [31] and Innerhofer et al. [32] described a passively mode-locked high-power RGB laser source based on a thin disc cut from an Yb:YAG crystal, which operated at a wavelength λ = 1030 nm and generated 705-fs pulses with an average power of 80 W at a repetition rate of 57 MHz. This configuration made it possible to substantially increase the output power and simplify the laser design because there were no laser amplifiers and the nonlinear conversion scheme was simplified. For example, the system employed regular domain structure crystals ($LiTaO_3$) operating at room temperature. Owing to the very high optical field intensities, parametric conversion was possible without synchronously pumped cavities. The average output powers of the RGB laser source at wavelengths λ_G = 515 nm, λ_B = 450 nm and λ_R = 603 nm were 23, 10.1 and 8 W, respectively. The IR to visible power conversion efficiency of this system is 51%. It is so far the most powerful laser colour source.

Another promising technology for making laser television projectors relies on the use of Novalux RGB lasers [33, 34]. These are Novalux extended cavity surface emitting lasers (NECSELs) (Fig. 3). Their cavity contains a $MgO:LiNbO_3$-based nonlinear element with a regular domain structure, which enables efficient intracavity frequency doubling.

Novalux managed to create RGB lasers emitting in a quasi-cw mode (f_{rep} = 500 Hz, τ_0 = 200 ns) at wavelengths λ_G = 532 nm, λ_B = 465 nm and λ_R = 620–635 nm. The average output power of each laser is 50–120 mW, with an overall efficiency in the range 5%–10%. Such lasers can readily be combined to form linear arrays. The total output power of linear arrays consisting of 14 individual lasers may reach 1.5 W. The use of linear arrays consisting of many indepen-

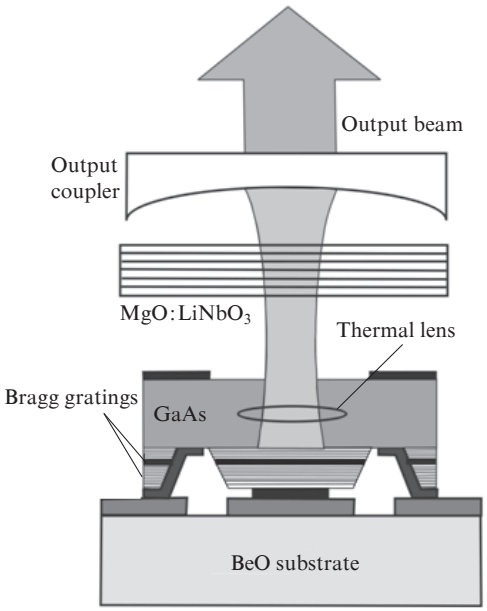

Figure 3. Schematic of the NECSEL.

dent laser oscillators allows one to substantially reduce the contrast of speckle structures in the image.

At the Consumer Electronics Show in January 2008, Mitsubishi Digital Electronics America officially presented the world's first commercial rear projection laser television system, which used Novalux lasers. In that system, light was modulated by an array of silicon micromirrors, referred to as a digital micromirror device (DMD), manufactured by Arasor (Australia), a company that relies on technologies developed by the Texas Instruments Company, which created a new type of imaging device – digital micromirror device. The array consists of 1920 × 1080 silicon mirrors 4 × 4 μm in dimensions. Each mirror is controlled by an electric voltage and has two stable positions, so the power of the light reflected from the mirrors is determined by the time the voltage is applied. According to its designers, the micromirror array ensures considerably higher image contrast than do liquid crystal modulators, which also can be used in this projection television system.

In our opinion, the television display system in question is not flawless. The time needed for the micromirrors to be switched from one position to the other is tens of microseconds, so dynamic image contrast must be not very high. Mirror sticking is possible. At high incident optical powers, heat removal from the crystalline material may pose a serious problem. The observed variation in image intensity is related to the physiology of human eye and has a cumulative character, which limits the use of these projectors in other applications, e.g. in high-speed real-time information display and recording systems.

Currently, the most attractive modulator for projection television information display systems with medium-power lasers, both pulsed and cw, is a linear micromechanical modulator consisting of an electrically controlled array of micromirrors produced by sputtering on movable silicon nitride (SiN) microsubstrates. This modulator fabrication technology is referred to as grating light valve (GLV) technology. It was first proposed in 1992 by Solgaard et al. [35] and was further improved by Bloom [36] and Trisnadi et al. [37]. The modulator may contain 4096 separately controllable pixels. Each pixel consists of two elements 3.7 × 200 μm in dimensions, one of which is controllable and can be moved within a quarter of the wavelength of incident light by an applied electric potential, and the other is fixed. When a voltage is applied to the controllable element, it shifts towards the substrate and the light deflects towards the projection optics. The reflected light intensity can be controlled by varying the time during which the light beams are in the deflected state. In contrast to the micromirror array, the switching time of one diffraction element in the GLV modulator is as short as 20 ns. The modulator allows one to obtain a one-dimensional amplitude-modulated line consisting of 4096 elements. Vertical scanning is planned to be performed using an electromagnetic galvanometer. According to the designers of the GLV modulator, at a refresh rate of 60 Hz one can obtain a 8192-line television raster. Currently, this modulator fabrication technology is planned to be used in producing small laser projectors for displaying television information from mobile phones.

At the present stage, it cannot be said that a universal method has been found and technology has been developed for fabricating information display and storage devices capable of resolving most practical issues. As a result of advances in science and technology, old technical solutions may turn out to be relevant at a new level. In our opinion, one such solution is pulsed television imaging using AOMs.

This approach offers the following advantages:

(1) possibility of imaging using only solid-state acousto-optic modulators and deflectors,

(2) absence of a high-speed mechanical horizontal scanning,

(3) high horizontal image linearity due to the constant speed of sound in the AOM crystal,

(4) ease of controlling and entering information,

(5) high speed of the system,

(6) possibility of controlling high-power laser beams,

(7) low sensitivity to external vibrations,

(8) simple optical imaging system,

(9) possibility of rapidly changing the image size and image–projector distance with no decrease in the number of resolvable elements and

(10) lack of a discrete image structure owing to the use of modulator arrays.

3. AOM for pulsed television display systems

An acousto-optic spatial light modulator for a pulsed line display system should meet a number of requirements. First, the length of the acousto-optic medium in the modulator should satisfy relation (1). This requirement limits the choice of the acousto-optic medium: on the one hand, by the small ultrasound velocity and, on the other, by the condition that the attenuation of ultrasonic waves over length L in the frequency range chosen be not high. Second, the modulator should ensure sufficiently effective control over the light beam, which implies that the acousto-optic medium should have a high acousto-optic figure of merit, M_2 [38], and a small absorption coefficient at the working wavelength. To reduce the reflection loss, one should have the possibility of coating the optical windows of the modulator with interference anti-reflection layers capable of withstanding exposure to a high-intensity laser beam. Third, the acousto-optic medium in the modulator should not have considerable phase inhomogeneities to avoid distortions of the wavefront of information-bearing light waves.

Analysis of existing acousto-optic media suggests that, at ultrasonic frequencies below 100–150 MHz, the above requirements are best met by paratellurite (TeO_2) crystals. This uniaxial material, transparent in the visible and near-IR spectral regions, possesses a variety of unique acousto-optic properties [39, 40]. In particular, the speed of slow ultrasonic shear waves in the [110] crystallographic direction is 0.616×10^3 m s^{-1}, which allows a modulated ultrasonic signal of 52-μs duration to be accommodated over a 32-mm-long segment in this direction.

The use of a slow ultrasonic shear wave for the diffraction of light from sound is possible in the case of anisotropic geometry of acousto-optic interaction. In the case of anisotropic scattering geometry, the wave vectors of the incident and diffracted light waves lie on different wave vector surfaces of the crystal, as distinct from those in isotropic geometry, and diffraction leads to rotation of the plane of polarisation of the light. Owing to the optical activity of TeO_2, when light propagates near its optic axis elliptically polarised waves are normal ones. As a result of anisotropic scattering, the ellipticity of the diffracted light waves and the azimuth of their polarisation ellipse depend on the ultrasound frequency,

and the rotation direction of their polarisation vector is opposite to that for the direct light. To effectively use the optical power in the case of acousto-optic interaction in a TeO_2 crystal, the polarisation of light incident on the crystal should be matched to the polarisation required for the scattering geometry chosen.

Figure 4 illustrates the geometry of acousto-optic interaction in a real device with pulsed line imaging for a TeO_2 AOM. Here a slow ultrasonic wave having a polarisation vector in the $[\bar{1}10]$ direction, parallel to the y axis, propagates through a TeO_2 crystal in the [110] direction. A light beam parallel to the diffraction plane $(\bar{1}10)$ impinges on the modulator. The angle between the beam wave vector and its projection onto the $(\bar{1}10)$ plane is α, and the angle between the projection of this vector onto the $(\bar{1}10)$ plane and the z axis is θ. The additional small angle α is introduced in order to take into account the effect of the input focusing lens on acousto-optic diffraction efficiency.

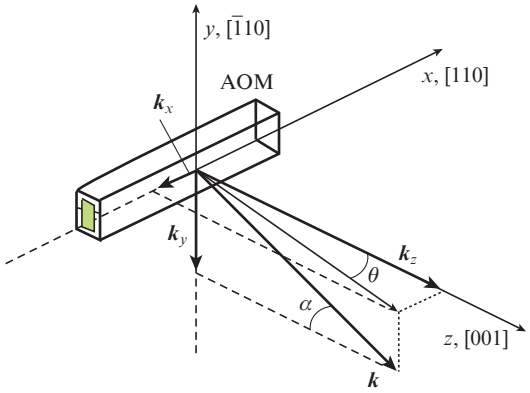

Figure 4. Geometry of acousto-optic interaction in a TeO_2 crystal.

TeO_2 crystals have highly anisotropic elastic and optical properties. Calculations demonstrate that, in the case of scattering from the $(\bar{1}10)$ plane of a TeO_2 crystal, anisotropic diffraction of light from a slow shear wave propagating in the [110] direction and small angles between the beam wave vectors and the optic axis of the crystal, the acousto-optic figure of merit M_2 exceeds that for fused silica by a factor of 793 (at a wavelength of 632.8 nm). This high efficiency allows one to use relatively low ultrasound powers (1 W or lower) to control acousto-optic devices. On the other hand, because of the strong anisotropy in the elastic properties of TeO_2, the faces of the acousto-optic crystal should be oriented with high accuracy. In particular, when the face with a piezoelectric transducer that excites a slow shear wave is 0.5° off the [110] axis in the (001) plane of a TeO_2 crystal, the energy flow of an elastic wave in the device deflects by 25° in this plane, which is the plane of the optical aperture of the AOM. As a result, at small ratios of the piezoelectric transducer height to the length of the crystal, there will be acousto-optic interaction only with part of the light incident on the modulator. A similar effect may arise from tapering of the intermediate bonding layers between the acousto-optic medium and piezoelectric transducer.

At a crystal length of 35 mm, the attenuation of a slow acoustic wave at a frequency of 80 MHz is 6–6.5 dB. Even though the attenuation coefficient of this type of ultrasonic wave is rather large (290 dB cm^{-1} GHz^{-2}), the natural gyrotropy of the crystal allows one to effectively use broadband anisotropic light scattering geometry at frequencies under 100 MHz.

At present, several laboratories in the world can grow high-quality TeO_2 crystals [41–43]. The length of a TeO_2 boule in the [110] crystallographic direction may reach 60–100 mm and its diameter may exceed 75 mm. When paratellurite single crystals are grown as described by Shakin et al. [42], there is no solarisation, which makes it possible to fabricate acousto-optic media with very low levels of light scattering. The scattering related to the surface processing of optical windows or spurious reflections in the crystal can be minimised. The quality of anti-reflection coatings achieved to date allows one to produce TeO_2-based AOMs with 99.5% transmission in the visible range.

According to optical damage resistance tests, TeO_2 crystals withstand periodic operation mode at pulse repetition rates from 1 to 3 Hz and incident laser intensities of up to 1 MW cm^{-2} [44]. Advances in the fabrication and design of TeO_2 modulators [45] have ensured that they have high stability to external influences such as mechanical vibrations, impacts, acceleration etc. When properly operated, the AOMs in question can serve for years.

An AOM includes a paratellurite crystal, which has two polished faces with anti-reflection coatings for laser wavelengths, and an X-cut lithium niobate piezoelectric transducer, attached to the end face of the crystalline cell by thermal-compression bonding. The transducer excites elastic shear vibrations in the frequency range of acousto-optic interaction. It has aluminium electrodes produced by sputter deposition. The top electrode of the piezoelectric transducer has the shape of an elongated hexagon in order to suppress acoustic side lobes. The cell is placed in a holder, which contains as well a device that matches the oscillator output to the piezoelectric transducer and a coaxial connector for delivering the electrical signal.

Figure 5 shows an acousto-optic cell for a television projection system [46], with a TeO_2 crystal, a piezoelectric transducer bonded to the crystal and sputter-deposited electrodes.

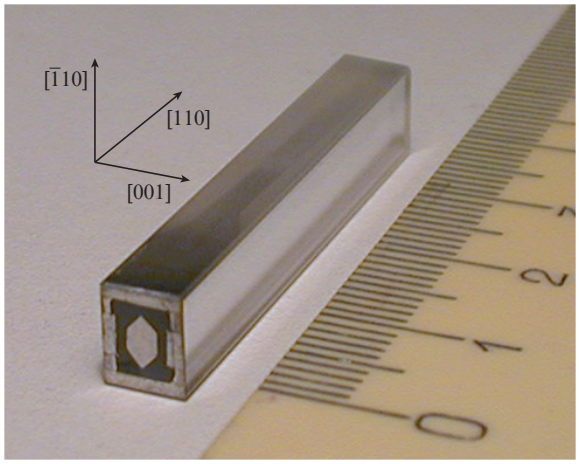

Figure 5. Photograph of the acousto-optic cell of an AOM in the form of a TeO_2 crystal with a piezoelectric transducer bonded to it and sputter-deposited electrodes.

The acousto-optic cell developed by Mokrushin and Shakin [18] was employed for television imaging [46, 47]. The cell uses diffraction in the $(\bar{1}10)$ plane, ensuring high diffraction efficiency, and allows an entire television line to be introduced into the modulator owing to the low speed of sound in it (616 m s^{-1}). The carrier frequency of ultrasound was 80 MHz, which made it possible to avoid two-phonon light scattering (57.9 MHz at a wavelength of 510.6 nm) at modulation frequencies under 20 MHz. The television line time is 64 μs. A part of the line, of 52-μs duration, contains information about the image, so the AOM length should be ∼32 mm.

As pointed out by Balakshii and Mantsevich [48], the unusually large acoustic beam divergence is associated with the insufficient accuracy in the fabrication of the samples studied and in the fabrication of the AOMs in the [110] direction for slow shear waves. The divergence is caused by the insufficient accuracy in the fabrication of the acousto-optic cell. Deviation of the modulator end face from the required crystallographic direction by 1′ causes the energy flow to deflect by about 1°. Mokrushin and Shakin [18] were able to overcome technological difficulties and ensure precision orientation of the (110) plane, to which a piezoelectric transducer was attached by thermal-compression bonding. They fabricated modulators that allowed a signal longer than 80 μs to be accommodated over the length of the crystal. As a result, at frequencies of the order of 100 MHz they observed no considerable acoustic beam divergence, which corresponded to the piston zone of the acoustic emitter at the corresponding aperture.

In a TeO_2 AOM, a slow elastic shear wave propagating in the [110] direction experiences strong attenuation. In order to equalise the amplitude of the ultrasonic wave along the length of the modulator, the line control unit should contain an attenuation compensator that provides a voltage which changes the gain coefficient of one of the power amplifier stages so that the amplitude of acoustic vibrations remains constant along the length of the AOM.

4. Characteristic features of image formation in an acousto-optic system with a pulsed coherent light source

The problem of diffraction of light from ultrasound has been the subject of extensive studies [49–55]. At present, there are two most general approaches to this problem, which allow one, in principle, to find a solution with predetermined accuracy. One approach is to solve a system of coupled differential difference equations describing interaction between different orders of diffraction. It was addressed in greatest detail in Refs [56–64]. The other approach is to solve an integral equation for a field obtained by introducing equivalent currents and expanding the sought field in terms of plane waves [65–68], which allows one to obtain an analytical solution for the diffracted field in the form of relatively rapidly converging series. Given that TeO_2 crystals are of practical interest, it is necessary to examine diffraction of light from ultrasound in an anisotropic medium with gyrotropic properties. Analysis of light diffraction in such a crystal is usually limited to the Bragg regime.

Mokrushin [69–71] found a generalised solution to the problem of diffraction in an anisotropic gyrotropic medium using a method proposed by Petrun'kin et al. [65–68], which eventually allows one to obtain an expression for the diffracted field after a TeO_2 AOM in the case of a harmonic amplitude modulation of a signal in an intermediate diffraction mode. Figure 6 presents an optical scheme that was used as the basis for a theoretical analysis of television image formation in an acousto-optic system with a pulsed laser [69–71]. It consists of an AOM, input cylindrical lens (L1) and objective lenses (L2, L3). The $x'z'$ and $y'z'$ planes of the system are chosen so that diffraction of light in the AOM and line image formation on the screen (S) take place in one of them (in the $x'z'$ plane), and line deflection in the plane of the screen takes place in the other. The diaphragm (D) located in the focal plane of lens L2 eliminates the zeroth order of diffraction, leaving only the light diffracted into the +1 order.

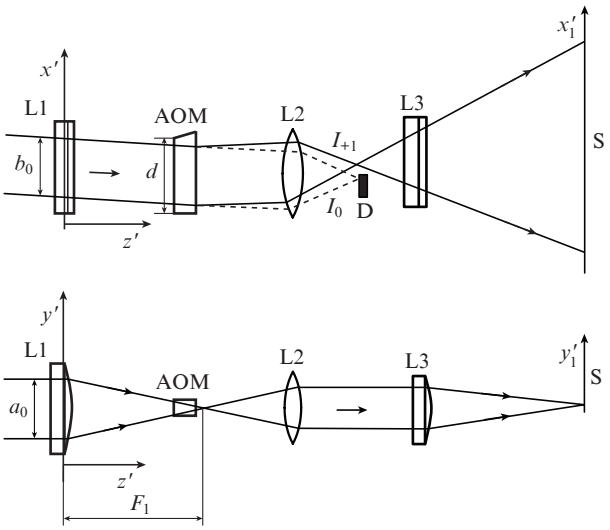

Figure 6. Optical schemes of the line imaging system in two mutually perpendicular planes: (L1) input cylindrical lens; (L2, L3) objective lenses; (D) diaphragm; (I_0, I_{+1}) intensities of the zeroth- and first-order beams; (a_0, b_0) beam dimensions along two axes; (F_1) focal length of lens L1; (d) size of the AOM along the x' axis.

Calculations were made for interaction geometry in a real device (Fig. 4), corresponding to broadband anisotropic diffraction of light from a slow elastic shear wave propagating through a TeO_2 crystal in the [110] direction. Mokrushin [69–71] calculated the time-averaged two-dimensional optical field intensity distribution in the image plane. He also calculated the modulation transfer characteristic of an acousto-optic line imaging system with a pulsed copper vapour laser and TeO_2 AOM for various optical pulse durations, ultrasound carrier frequencies, acousto-optic interaction lengths and angles of incidence of light on the AOM in a plane orthogonal to the diffraction plane. This allowed the effect of the input cylindrical lens on acousto-optic diffraction efficiency to be taken into account.

It was assumed that an amplitude-modulated ultrasonic signal was fed to the AOM input, with an amplitude

$$A(\boldsymbol{r}) = A_0\left[1 + m_0\cos\left(2\pi f_0 \frac{\boldsymbol{r}}{\boldsymbol{v}}\right)\right] = A_0[1 + m_0\cos(\Phi_0 x)], \quad (4)$$

where m_0 is the modulation depth; f_0 is the modulation frequency; $\boldsymbol{v}$ is the velocity vector; and $\boldsymbol{r}$ specifies the pro-

pagation direction of the ultrasonic perturbation in the medium.

Assuming that the Bragg diffraction conditions were strictly satisfied for the central spectral component of the amplitude-modulated signal and taking into account only interactions between the +1 and zeroth orders of diffraction, he calculated the +1 diffraction order field at the boundary of the ultrasonic column in the TeO_2 AOM and the time-averaged light intensity in the line on the screen. The field was calculated according to a scattering diagram that represented successive events of light diffraction from spectral components of an ultrasonic wave. Deviations from the Bragg conditions were taken into consideration by taking into account the acoustic beam divergence. Figure 7 shows such a diagram in the third-order interaction approximation. Final calculations were performed to accuracy of the fifth order in interaction inclusive.

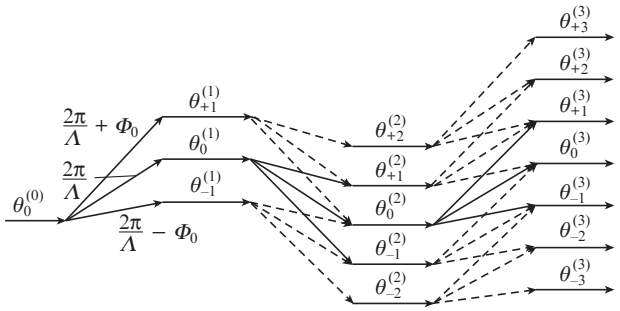

Figure 7. Scattering diagram for diffraction of light into the +1 order in the third-order interaction approximation. Λ is the acoustic wavelength.

The horizontal arrows in the diagram correspond to partial plane waves propagating at angles $\theta_p^{(m)}$ for orders of interaction $m = 0-3$. The slanted arrows indicate the possible directions of scattering of these waves under the effect of ultrasonic perturbation. It follows from the diagram that, in the third-order interaction approximation, a signal with three spectral components has 27 possible scattering geometries contributing to the diffracted field near the +1 order. The spectrum of this field consists of seven components with different diffraction angles $\theta_p^{(3)}$ and frequencies differing by $\Delta\Omega_p = p2\pi f_0$, where $p = -3, -2, -1, 0, +1, +2, +3$. The calculations took into account the ellipticity of each spectral component of the diffracted light waves.

In the third-order interaction approximation, the time-averaged light intensity distribution in the line on the screen along the x_1' axis for a Gaussian pulse shape has the form

$$I_1(x_1') = \tilde{I}_0\chi_0^2\left\{C_0 + 2\sum_{n=1}^{6}\left[C_{n1}\cos\left(\frac{2\pi n f_0 x_1'}{v}\right) + C_{n2}\sin\left(\frac{2\pi n f_0 x_1'}{v}\right)\right]\exp\left[-\left(\frac{\pi n f_0 \tau_0}{2\sqrt{\ln 2}}\right)^2\right]\right\}, \quad (5)$$

$$\tilde{I}_0 = \frac{c\tau_0 a_0^2 E_0^2}{16\lambda_0\sqrt{\pi\ln 2}\, M_1' M_2' TF_1}, \quad (6)$$

where T is the pulse repetition period; τ_0 is the optical pulse width at half maximum; E_0 is the electric field intensity of the light wave in air; M_1' and M_2' are the horizontal and vertical magnifications of the optical system; λ_0 is the wavelength of the light in vacuum; and χ_0 is the modulation index. The coefficients C_0, C_{n1} and C_{n2} depend on the $\theta_p^{(m)}$ angles, m_0, the ellipticity of partial light waves and the modulation index:

$$\chi_0 = \frac{\pi A_0 \xi^{(0)} n_o^3 L(p_{11} - p_{12})}{2\lambda_0}, \quad (7)$$

where $\xi^{(0)}$ is the normalised strain of the medium; n_o is the index of refraction for an ordinary light wave; L is the acousto-optic interaction length; and p_{11} and p_{12} are the photoelastic constants of TeO_2.

The first term in (5) represents the constant component of the image signal. In addition to the terms containing C_{11} and C_{12}, which describe modulation at the fundamental frequency f_0, the image signal will contain terms with higher harmonics, up to the sixth harmonic of the input signal, which will distort it.

A distinctive feature of the operation of an AOM in television imaging is substantial nonlinearity of its amplitude transfer characteristic, which reduces the working dynamic range of the system and distorts the optical signal at high diffraction efficiencies.

Figure 8 presents characteristic dependences of the diffraction efficiency $I(\chi_0) = I_{+1}^{\max}/(I_{+1}^{\max} + I_0^{\max})$ at image signal maxima on the modulation index χ_0, for an ultrasonic signal (4) with a harmonically modulated amplitude at different modulation frequencies f_0 and acousto-optic interaction lengths L. Figure 9 shows the measured relative light intensity at the image signal maximum vs. the amplitude U_s of an input harmonic signal with a carrier frequency $f = 82.5$ MHz at different ultrasound modulation frequencies. Comparison of the data in Figs 8 and 9 at high signal amplitudes demonstrates qualitative agreement.

Theoretical and experimental examination of the image formation process in an acousto-optic system with a pulsed coherent light source indicates that, at high ultrasonic signal amplitudes, the image is distorted, which is caused by light rediffraction to higher diffraction orders of the modulation signal and leads to broadening of the energy spectrum of the image signal. With increasing amplitude, the spectrum of the image signal changes: additional components emerge due to the nonlinearity of light diffraction by ultrasound. Increasing the ultrasonic signal amplitude increases the fraction of the optical energy in these components and distorts the symmetry of the spectrum with respect to the central component. At high modulation indices, the distortion of the image depends on the modulation frequency, optical pulse duration and acousto-optic interaction length. In the case of central tuning (the Bragg conditions are satisfied for the central spectral component of the amplitude-modulated signal), at low modulation frequencies the side components are located near the ultrasound carrier frequency. At these frequencies, the conditions for rediffraction and, hence, for the formation of side components at frequencies that are multiples of the modulation frequency are easier to satisfy. The shape of a harmonic image signal then becomes distorted, approaching a rectangular one. Figure 10 illustrates the effect of the modulation index on the calculated shape of a harmonic image signal

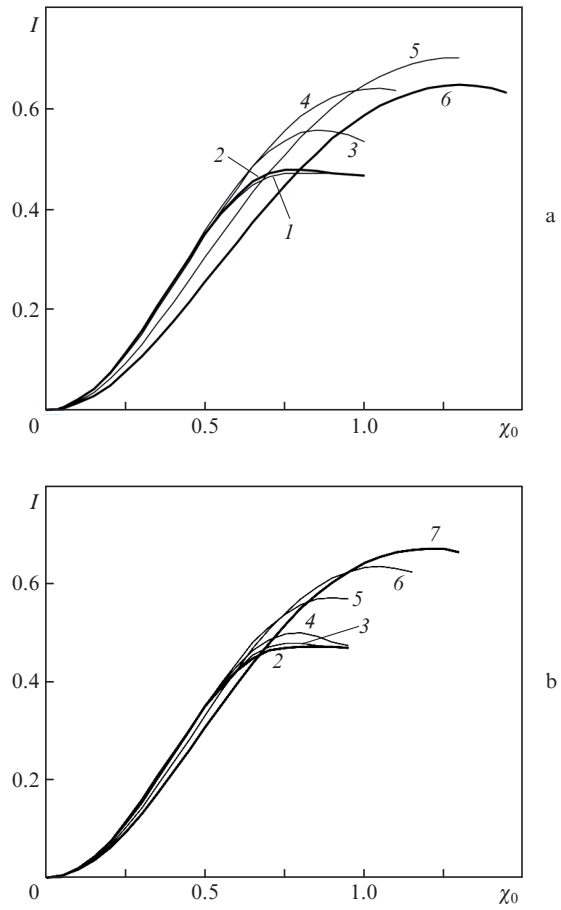

Figure 8. $I(\chi_0)$ dependences of diffraction efficiency at image signal maxima at L = (a) 6 and (b) 2 mm, λ_0 = 510.6 nm, f = 80 MHz, τ_0 = 10 ns and modulation frequencies f_0 = (*1*) 0.5, (*2*) 1, (*3*) 3, (*4*) 5, (*5*) 10, (*6*) 15 and (*7*) 20 MHz.

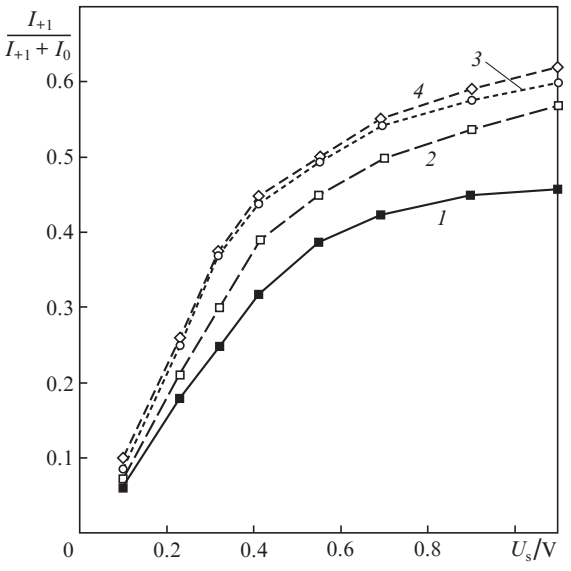

Figure 9. Measured relative light intensity at the image signal maximum vs. the amplitude U_s of an input harmonic signal with a carrier frequency f = 82.5 MHz at ultrasound modulation frequencies f_0 = (*1*) 1, (*2*) 3, (*3*) 5, and (*4*) 10 MHz.

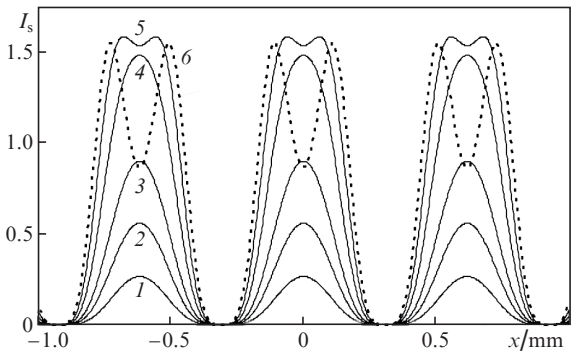

Figure 10. Variations in the shape of a harmonic image signal at a modulation frequency f_0 = 1 MHz and modulation indices χ_0 = (*1*) 0.2, (*2*) 0.3, (*3*) 0.4, (*4*) 0.6, (*5*) 0.8 and (*6*) 1.0.

$I_s(x) = I_1(x)/\tilde{I}_0$ at a modulation frequency of 1 MHz. With increasing modulation index, the increase in peak intensity drops sharply because the optical field energy is effectively transferred to the diffraction components at frequencies that are multiples of the modulation frequency.

At higher f_0 frequencies, the spectral components of the diffracted optical field that correspond to rediffraction have a substantially lower amplitude than at low frequencies because of the limited acousto-optic interaction band, and a smaller fraction of the optical field energy is transferred to them as a result of diffraction. The signal shape is less distorted, and the light intensity at the image signal maximum increases with increasing ultrasonic signal amplitude. At high f_0 frequencies, the decrease in $I(\chi_0)$ is caused by the finite width of the acousto-optic interaction band. Less energy is then transferred to the side components, which leads to a reduction in image contrast and, eventually, to complete loss of the information about the ultrasonic signal modulation. In this case, the image on the screen has the form of a uniform illumination with an intensity corresponding to the amplitude of the central component of the signal.

This effect can be observed in experiments. It is undesirable and limits the permissible light diffraction efficiency at low modulation frequencies. To increase the optical power utilisation factor of the laser source, amplitude correctors should be introduced into the video signal amplification channel in order to equalise the nonlinearities of the amplitude characteristics of the AOM at different frequencies. The transfer characteristic of the correctors should have the form $U_2 = F^{-1}(U_1)$, where $F^{-1}(x)$ is the inverse function of $F(x)$. Exact correction in a wide range of modulation frequencies is difficult to ensure for an AOM. One can, for example, divide the video signal channel in the corrector into several parallel frequency channels covering the entire frequency spectrum of the input signal, each with its own correction law for nonlinearity in the transfer characteristic. Next, the signals are added together. In doing this, one must equalise the phase delays of the signals in each channel. With such correction, the laser output power will be utilised more efficiently.

It is worth noting that, in the case of image formation along a line, there are no special requirements for the coherence and spectral purity of the laser radiation, because the purpose is to image the ultrasonic field in the AOM. The only requirement is the possibility of eliminating the zeroth and

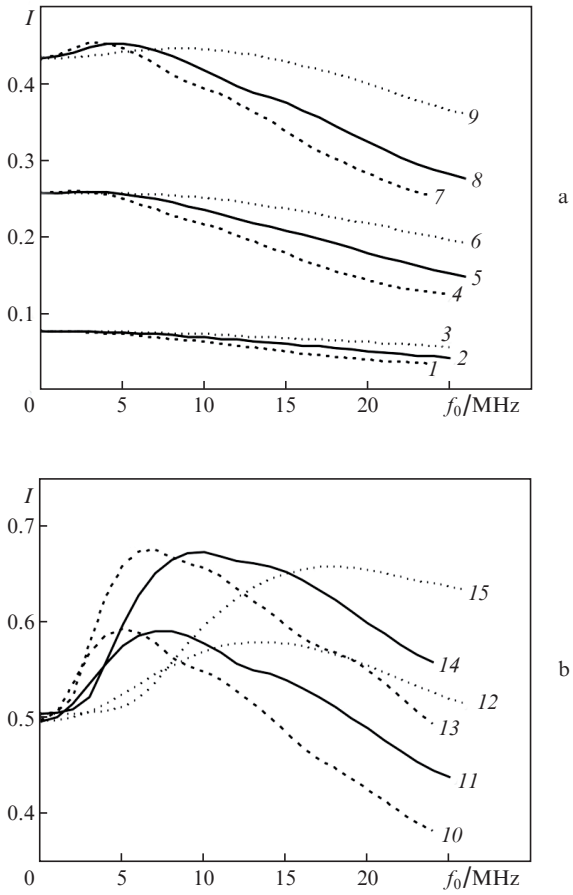

Figure 11. Diffraction efficiency at image signal maxima, $I(\chi_0)$, in the fifth-order interaction approximation vs. modulation signal frequency f_0: (a) L = 6, 4 and 2 mm and χ_0 = (*1–3*) 0.2, (*4–6*) 0.4 and (*7–9*) 0.6; (b) L = 6, 4 and 2 mm and χ_0 = (*10–12*) 0.8 and (*13–15*) 1.0.

spurious diffraction orders by a diaphragm (D). At the same time, in the vertical scanning direction on the screen one should obtain an image of the optical beam waist, so there are stringent requirements for the spatial coherence of the laser radiation in this direction. The real number of resolvable elements per frame will depend on the actual width of the laser radiation directivity diagram and the factors that broaden it after light propagation through the optical forming system. In addition to large angles of incidence on the AOM in the plane orthogonal to the diffraction plane, such factors may include nonuniformities of the refractive indices of the optical components of the system, which distort the light wavefront, and a nonuniform optical field distribution on the output deflector aperture, which may result e.g. from nonuniform illumination of the aperture by incident light or from the variation in diffraction efficiency due to the decay of the elastic wave.

Figure 11 shows the calculated diffraction efficiency at image signal maxima, $I(\chi_0) = I_{+1}^{\max}/(I_{+1}^{\max} + I_0^{\max})$, as a function of modulation signal frequency f_0 at different modulation indices χ_0 and acousto-optic interaction lengths L. $I_{+1}^{\max}$ was calculated in the fifth-order interaction approximation, and $I_0^{\max}$, in the fourth-order approximation. These data can be regarded as the amplitude–frequency response of the optical image formation system with a pulsed laser and TeO_2 AOM.

It is seen in Fig. 11 that, with decreasing L, the diffraction efficiency in the high-frequency region and the acousto-optic interaction bandwidth increase. At the same time, with increasing L the diffraction efficiency increases in the low-frequency region and the working frequency range of the system decreases. At high modulation indices, diffraction efficiency varies little at low frequencies (0.1–1 MHz), because the amplitude is limited by optical energy transfer to high harmonics of the modulation signal. Diffraction efficiency is limited by a level of ~0.5 at modulation frequencies under 1 MHz.

Figure 12 shows the diffraction efficiency at image signal maxima, $I(\chi_0)$, for fifth-order interaction at different modulation signal frequencies f_0 and optical pulse durations τ_0 (L = 4 mm). These data represent amplitude transfer characteristics of the system. It is seen that, to image an amplitude-modulated ultrasonic signal with a bandwidth of 5–7 MHz (standard television signal), it is quite sufficient to use lasers with an optical pulse duration $\tau_0 \simeq 30 - 40$ ns.

As a result of the increase in the bandwidth of the video signal at long optical pulse durations, diffraction efficiency drops sharply at high frequencies. This is accompanied by a decrease in the contrast of these spectral components. The optical image intensity increases only through an increase in power at the carrier frequency of the signal.

When the carrier frequency of ultrasound is modulated by an input signal with a complex spectrum, nonlinear distortions of the image signal at large ultrasound amplitudes are considerably more difficult to analyse. As a result of the first-order diffraction by sound, the optical fields will contain frequency components shifted in frequency according to the spectrum of the modulation signal. As a result of rediffraction, each frequency component has multiple frequencies according to the order of acousto-optic interaction, and the corresponding amplitudes are nonlinear functions of the modulation index. Further, in the image plane all the fields are added together to form anintensity distribution that contains – on account of the field multiplication – additional harmonics of the fundamental frequencies of the spectrum and combination components. The increase in the intensity of the combination components of the second or higher order will be determined by rediffraction processes and will be accompanied by energy transfer to spectral components with multiple harmonics of the modulation frequencies of the input signal. Because of this, the calculated modulation indices χ_0 starting at which nonlinear distortion of the signal increases sharply will be the same for one modulation frequency and a signal with a complex spectrum. To obtain small distortions in the image signal, it is probably necessary that the modulation indices of all spectral components of the input modulation signal not exceed the permissible value of χ_0 for their frequency.

5. Vertical beam scanning devices

The selection of a vertical beam deflection device depends on the requirements for the entire information display system. The characteristics determining the operation of such a device include the number of resolvable elements, deflection linearity, efficiency and the possibility of superposing images at different wavelengths. The number of resolvable elements at the output of any deflector is given by

$$N_{\text{fr}} = \Delta\varphi_{\text{sc}}/\Delta\Psi_0, \tag{8}$$

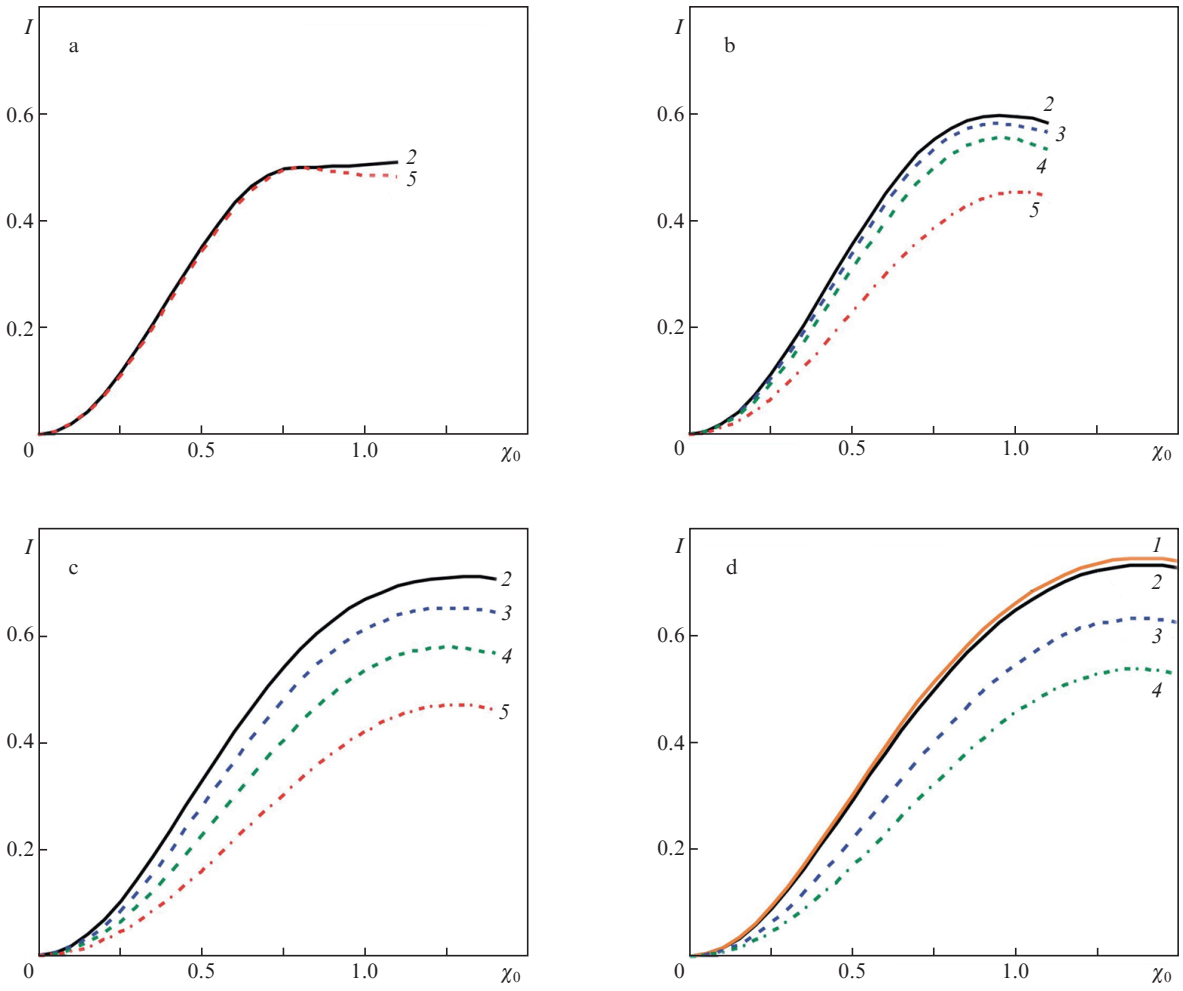

Figure 12. Diffraction efficiency at image signal maxima, $I(\chi_0)$, in the fifth-order interaction approximation at optical pulse durations τ_0 = (*1*) 5, (*2*) 10, (*3*) 30, (*4*) 50 and (*5*) 100 ns and modulation frequencies f_0 = (a) 1, (b) 5, (c) 10 and (d) 15 MHz.

were $\Delta\varphi_{sc}$ is the scan angle and $\Delta\Psi_0$ is the light beam divergence at the deflector output.

In the case of electromechanical deflectors (mirror galvanometers, rotating polygon mirrors), the scan angle may reach several tens of degrees. At a near diffraction-limited light beam divergence, the number of resolvable elements per frame may reach several thousand. If the desired resolution is not so high as, e.g. in the 625 line television standard, use can be made of light beams with a divergence considerably exceeding the diffraction limit. When electromagnetic mirror galvanometers are used, one should ensure not only high linearity and stability of forward scanning but also rapid return of the mirror to its initial state, within the frame blanking pulse duration (1.6 ms or less). At present, a wide variety of electromagnetic galvanometers with characteristics suitable for laser beam deflection are available (manufactured by Cambridge Technology Inc., General Scanning Inc. and GSI Lumonics).

AODs are convenient for vertical light beam deflection because they do not contain mechanically moving parts or units sensitive to mechanical vibrations or pressure differences and also because they offer the possibility of fast electronic control over beam scanning parameters. An important advantage of AODs over electromagnetic galvanometers is the considerably shorter light beam flyback time. In the case of AODs, the flyback time is determined by the time needed for an acoustic wave to traverse the acousto-optic cell and is just a few tens of microseconds. The scan angle of AODs does not exceed a few degrees, so, when using such a deflector, one should minimise the laser beam divergence and take into account all the mechanisms responsible for the broadening of the laser radiation directivity diagram along the *y* axis. In calculations of an optical system, the thickness of the acousto-optic medium of the AOD should also be taken into account.

At a fixed $\Delta\varphi_{sc}$ angle, the maximum number of resolvable elements at the AOD output can be obtained at a diffraction-limited divergence of the laser beam incident on the deflector and a uniform distribution of the diffracted field over the rectangular output aperture:

$$N_{fr} = D\Delta\varphi_{sc}/\lambda_0, \tag{9}$$

where D is the size of the aperture of the deflector in the scattering plane. If the field distribution in the output beam of the deflector is nonuniform, in particular as a consequence of the decrease in diffraction efficiency because of the decay of the elastic wave, the limiting resolution is lower, as shown e.g. by Molotok and Razzhivin [72].

The scan angle can be determined by jointly solving equations representing the laws of conservation of energy and momentum for interacting optical and acoustic waves in the crystal [73]. For geometric interpretation of the solution, it is convenient to use vector scattering diagrams. Every vector diagram corresponds to a limiting case of diffraction theory in which the Bragg condition is satisfied for both the incident and diffracted light waves:

$$\boldsymbol{k}_\mathrm{d} = \boldsymbol{k}_\mathrm{i} + \boldsymbol{k}_\mathrm{snd}, \tag{10}$$

where $\boldsymbol{k}_\mathrm{i}$, $\boldsymbol{k}_\mathrm{d}$ and $\boldsymbol{k}_\mathrm{snd}$ are the wave vectors of the optical and acoustic waves.

From the vector scattering diagram, we find relations between the magnitudes of the wave vectors of the incident beam, $\boldsymbol{k}_\mathrm{i} = (2\pi/\lambda_0)n_\mathrm{i}$, and diffracted beam, $\boldsymbol{k}_\mathrm{d} = (2\pi/\lambda_0)n_\mathrm{d}$, in the crystal, the angle of incidence θ_i, the diffraction angle θ_d and the wave vector of the elastic wave, $\boldsymbol{k}_\mathrm{snd} = (2\pi f/v)\boldsymbol{r}$, where the vector $\boldsymbol{r}$ specifies the elastic wave direction. A change in one of the quantities in the vector triangle leads to changes in the others.

In the case of AODs, use is typically made of operation conditions under which the direction and magnitude of the wave vector of incident light, $\boldsymbol{k}_\mathrm{i}$, remain constant, and the direction of the diffracted light beam is controlled by varying the frequency and direction of the ultrasonic wave. It is most easy to produce the required change in the direction of the ultrasonic wave at low frequencies owing to the diffraction-limited divergence of the acoustic beam. Usually, the frequency of the ultrasonic signal fed to an AOD for vertical laser beam deflection varies linearly.

Specific features of acousto-optic interaction geometry in different crystal systems have been the subject of many studies (see e.g. Refs [74, 75]). It was pointed out in all those studies that deflectors employing anisotropic diffraction of light had some advantage over those employing isotropic diffraction. The advantage is that, near the frequency

$$f_\mathrm{d} = \frac{v}{\lambda_0}\sqrt{|n_\mathrm{e}^2 - n_\mathrm{o}^2|},$$

the required range of deflection angles can be reached at a lower ultrasonic wave divergence and, hence, at lower energies. In examining anisotropic deflectors, many groups [76, 77] pay special attention to TeO_2 deflectors, which allow for a broadband scattering geometry at rather low ultrasound frequencies, in the range 50–100 MHz, with high diffraction efficiency (70%–80%). As a rule, the range of acoustic frequencies used does not exceed one octave in order to prevent the second order of diffraction from falling into the scan range.

The maximum number of resolvable elements in such deflectors can be found as

$$N_\mathrm{fr} = \Delta f D/v. \tag{11}$$

For a deflector with $D = 15$ mm, $\Delta f = 50$ MHz and $v = 0.65 \times 10^3$ m s^{-1}, we obtain from the Rayleigh criterion $N_\mathrm{fr} \simeq 1154$, which is quite acceptable for information display systems operating in an enhanced-definition standard.

For effective AOD operation, the parameters of the light beam should meet certain requirements. In particular, in the vertical deflection plane the light beam incident on the deflector should be parallel, its dimensions should correspond to those of the acoustic beam in the AOD crystal, and the polarisation of the incident light should correspond to that required for the acousto-optic interaction geometry chosen. An important issue in designing AODs is the uniformity and width of the acoustic beam within the working aperture of the deflector. To obtain an undistorted image on a screen, the deflector should ensure equally effective deflection of light beams related to the diffraction components that form the image. The working aperture of an AOD, determined by the width of the sound column in the deflector, acts as a filter of spatial frequencies and determines the passband of the television image formation system.

6. Optimisation of pulsed laser output parameters with application to a projection information display system

A theoretical analysis of the line image formation process in an acousto-optic system with a pulsed laser suggests that the quality of reproduced information should be significantly influenced by laser output parameters such as the beam divergence and laser pulse duration. A long laser pulse duration should lead to a decrease in the maximum number of resolvable elements and the contrast in amplitude-modulated signal imaging. Laser beam divergence should match the capabilities of the light deflector used in the system. If an AOD is used in the system, the beam divergence should be near diffraction-limited. Moreover, to ensure effective utilisation of optical power the polarisation of laser light incident on an AOM should correspond to the eigenmode of the light wave propagating in the acousto-optic medium of the AOM.

The main requirements that should be taken into account in choosing lasers for a pulsed television display system are as follows:

(1) pulsed lasing with a pulse repetition rate equal to the television line rate,

(2) short laser pulse duration according to (2),

(3) sufficiently high average output power of the laser,

(4) beam polarisation matched to the eigenmode of light wave in the AOM and

(5) the possibility of producing a full-colour RGB laser source.

The development of a laser meeting all the above requirements is a priority issue, which should be resolved in designing an information display based on pulsed line imaging.

7. Pulsed lasers for a television display system

7.1. Gas lasers

Historically, the first lasers best suited for pulsed television imaging were self-terminating metal vapour lasers [78], which are still among the most powerful coherent light sources in the visible range [79–81]. To date, lasing has been obtained and lasers have been made using transitions of various metals, and many of the corresponding lines lie in the visible range.

The best energy performance is offered by the copper vapour laser, which operates at two wavelengths: λ_1 = 510.6 nm and λ_2 = 578.2 nm. Typical laser pulse durations lie in the range 5–30 ns, and the pulse repetition rate ranges from 8 to 30 kHz, which corresponds to television line rates. The average output power of this laser in a master oscillator/power amplifier system may reach hundreds of watts, with 1% efficiency. A red colour for a television information display system can be obtained using a gold vapour laser (λ = 627.8 nm). Even though bismuth vapour (λ = 472.2 nm) [82] and iron vapour (λ = 452.9 nm) [83] have been demonstrated to lase, the question of whether it is possible to create a sufficiently efficient pulsed self-terminating blue laser close in output characteristics to the copper and gold vapour lasers remains open.

High gain and short inversion lifetimes in the active medium lead to difficulties in producing lasers with high light directivity, which is necessary e.g. in projection television information display systems. Beam divergence can be reduced, down to the diffraction limit, by using an unstable laser cavity with a large gain coefficient [84]. Note that a decrease in beam divergence by an order of magnitude relative to a stable-cavity laser leads to a reduction in output power by about 30%. High output power in combination with high output directivity can be achieved in a master oscillator/power amplifier system [85].

Unfortunately, the choice of sufficiently powerful self-terminating metal vapour lasers for information display systems in the visible range is currently limited to the copper and gold vapour lasers. The other metal vapour lasers have low efficiency.

7.2. Solid-state lasers

Recent years (from the end of the 20th century to the beginning of the 21st) have seen rapid advances in pulsed solid-state lasers and laser systems with nonlinear conversion of IR radiation to the visible range. Diode-pumped solid-state lasers have attracted considerable attention owing to their small dimensions, long service life and high overall efficiency. Controlled pulsed operation of such lasers can be ensured by intracavity Q-switching using electro-optical or acousto-optic Q-switches. The simplest approach for obtaining pulsed radiation in the visible range is intracavity second or third harmonic generation. In particular, Du et al. [86] demonstrated intracavity Nd:YVO_4 laser (λ = 1342 nm) frequency doubling using a BBO nonlinear crystal. The average output power at λ = 671 nm was 4.38 W, with f_{rep} = 70 kHz, τ_0 = 290 ns and conversion efficiency of 9.5%.

They also reported intracavity Nd:$GdVO_4$ laser frequency doubling using a BBO nonlinear crystal [87]. The average output power at λ = 671 nm was 6 W, with f_{rep} = 47 kHz, τ_0 = 97 ns and conversion efficiency of 12.8%. The beam quality factor was M^2 = 2.47 and the output power stability was 5.8%.

Using intracavity sum frequency mixing of the fundamental and second harmonics of an acousto-optically Q-switched Nd:$YAlO_3$ (Nd:YAP) laser, Haiyong et al. [88] obtained light at λ = 447 nm. The second harmonic was generated in an LBO crystal and the sum frequency was generated in a $KTiOPO_4$ (KTP) crystal. The average output power at λ = 447 nm was 4.46 W, with f_{rep} = 4.6 kHz and τ_0 = 190 ns. The output power stability was 3% over a period of 1 h.

Konno et al. [89] reported the highest output power (138 W) of the second harmonic (λ = 532 nm) of a diode-pumped Q-switched Nd:YAG laser at a pulse repetition rate of 10 kHz and pulse duration of 70 ns. Intracavity frequency doubling was ensured by an LBO nonlinear crystal. The conversion efficiency from the diode pump (λ = 808 nm) to the laser beam (λ = 532 nm) was 17.3%, at an overall laser efficiency of 7.9%. The optical power density at the laser beam waist was 434 MW cm^{-2}, the beam quality factor was M^2 = 11, and the output power stability was 3% over a period of 200 h. Bo et al. [90] improved the output characteristics of this laser: they obtained an output power of 120 W at f_{rep} = 10 kHz, τ_0 = 80 ns and M^2 = 6.2.

The relatively long pulse duration of such lasers is due to the use of AOMs for Q-switching. Shorter laser pulses can be obtained using EOMs. For example, Tang et al. [91] reported a prototype Q-switched diode-pumped Nd:YVO_4 solid-state laser operating at a pulse repetition rate f_{rep} = 20 kHz with intracavity frequency doubling in an LBO crystal. They obtained a laser pulse duration τ_0 = 10 ns owing to the use of a $La_3Ga_5SiO_{14}$ (LGS) EOM as a Q-switch. The average laser output power at λ = 532 nm was 2.3 W, with a maximum optical conversion efficiency of 9.6%. The best beam quality ($M^2 < 2$) was obtained at P_{out} = 1.5 W. The output power stability was then 1.4% or better.

More complex systems for conversion of the IR radiation of solid-state lasers are those employing nonlinear parametric light conversion. Lee and Moulton [92] and Moulton et al. [93] used a diode-pumped (λ = 805 nm) neodymium-doped yttrium lithium fluoride (Nd:$YLiF_4$) solid-state laser as a fundamental frequency source. The laser comprised a Q-switched master oscillator and two amplifier stages on the same crystal. Q-switching was ensured by an AOM. The output of the fundamental source was frequency-doubled in an LBO nonlinear crystal. The output parameters were as follows: average output power P_{out} = 30 W at λ = 524 nm, pulse repetition rate f_{rep} = 22.5 kHz, optical pulse duration τ_0 = 35 ns, beam quality factor $M^2 < 1.2$. The radiation was then converted in a nonlinear optical scheme comprising an optical parametric oscillator and two LBO crystal doublers. The output of the system was laser radiation at three wavelengths, 524 (P = 5.8 W), 628 (P = 6 W) and 449 nm (P = 3.5 W), which could be used in a full-colour television projector with a luminous flux of 4000 lm. The wall-plug power of the entire laser system was 365 W, with an overall efficiency of 11%.

The solid-state lasers have small dimensions, high overall efficiency and a long operating life (up to 10^4 h) compared to the metal vapour gas lasers. Nevertheless, they are inferior in some output characteristics of considerable importance for projection information display systems with pulsed lasers: these are, first of all, the high level of laser output power fluctuations and the optical pulse duration (~100 ns) being not short enough for high-power Q-switched solid-state lasers.

8. Characteristic features of television image formation in an acousto-optic system with a pulsed laser

In designing an optical system with a pulsed projection of an amplitude-modulated line, the following factors should be taken into account:

In the optical scheme shown in Fig. 6, the AOM is located in the focal plane of the cylindrical lens. Because of this, when high laser output powers are used, the power density at the beam waist reaches high levels, which may lead to local heating and disturb the optical uniformity of the acousto-optic medium. This in turn would degrade the parameters of the television line being projected, i.e. reduce the number of resolvable elements and limit the dimensions and brightness of the image. In the limit of low laser beam divergence, the acousto-optic medium may be damaged. Moreover, since the acousto-optic medium is located at the laser beam waist, which coincides with the object plane of the projection objective, the projection system is extremely sensitive to various refractive index nonuniformities in the acousto-optic medium and modulator windows, which show up as vertical bands in the image.

Another characteristic feature of the system under consideration is the concurrent operation of the laser at several wavelengths, which can be used in image formation. For example, the copper vapour laser emits at two wavelengths, $\lambda_1 = 510.6$ nm and $\lambda_2 = 578.2$ nm, with roughly equal average output powers in the case of steady-state heating of the gain element. When a TeO_2 AOM is tuned to the maximum diffraction efficiency at one of these wavelengths (λ_1) at a particular ultrasound frequency f and an angle of incidence θ'_{i1}, the conditions for efficient diffraction of light at the other wavelength at this angle of incidence are not satisfied or are satisfied for part of the frequency band of the modulation signal. As a result, when one AOM is used for imaging, one has to use only one wavelength of the copper vapour laser, thereby considerably reducing the light usage efficiency.

Note also that the instant when the spectral component of wavelength λ_2 in the copper vapour laser reaches its peak power lags that for the spectral component λ_1 by a time $\Delta\tau_0 \approx 10-20$ ns, depending on the conditions under which the gain element is pumped. During this time, the ultrasonic wave in the AOM travels a distance $\Delta l = \Delta\tau_0 v$. As a result, the light replicas of the television line signal at the output of the AOM for components at different wavelengths will be shifted relative to each other.

To eliminate these drawbacks to the optical scheme of a projection device presented in Fig. 13, a linearly polarised parallel laser beam is directed at 45° in the horizontal plane on a dichroic mirror (M1), which reflects the λ_1 spectral component of the beam and transmits the λ_2 component.

The λ_2 spectral component of the laser beam impinges on mirror M2 at an angle $45°-\beta$ and, after reflection, passes again through mirror M1. Thus, the system of mirrors M1 and M2 splits the laser beam into two components of wavelengths λ_1 and λ_2, which propagate at an angle 2β to each other. Next, the two beams pass through a laser light polarisation converter C (Fresnel rhomb), which converts their linear polarisations to elliptical (nearly circular), so that they approach the eigenpolarisations of the light waves incident on the acoustic beam in the TeO_2 crystal of the AOM.

After the polarisation converter C, the laser beam passes through a laser beam aperture converter consisting of lenses L3, L4 and L5, which changes the dimensions of the parallel

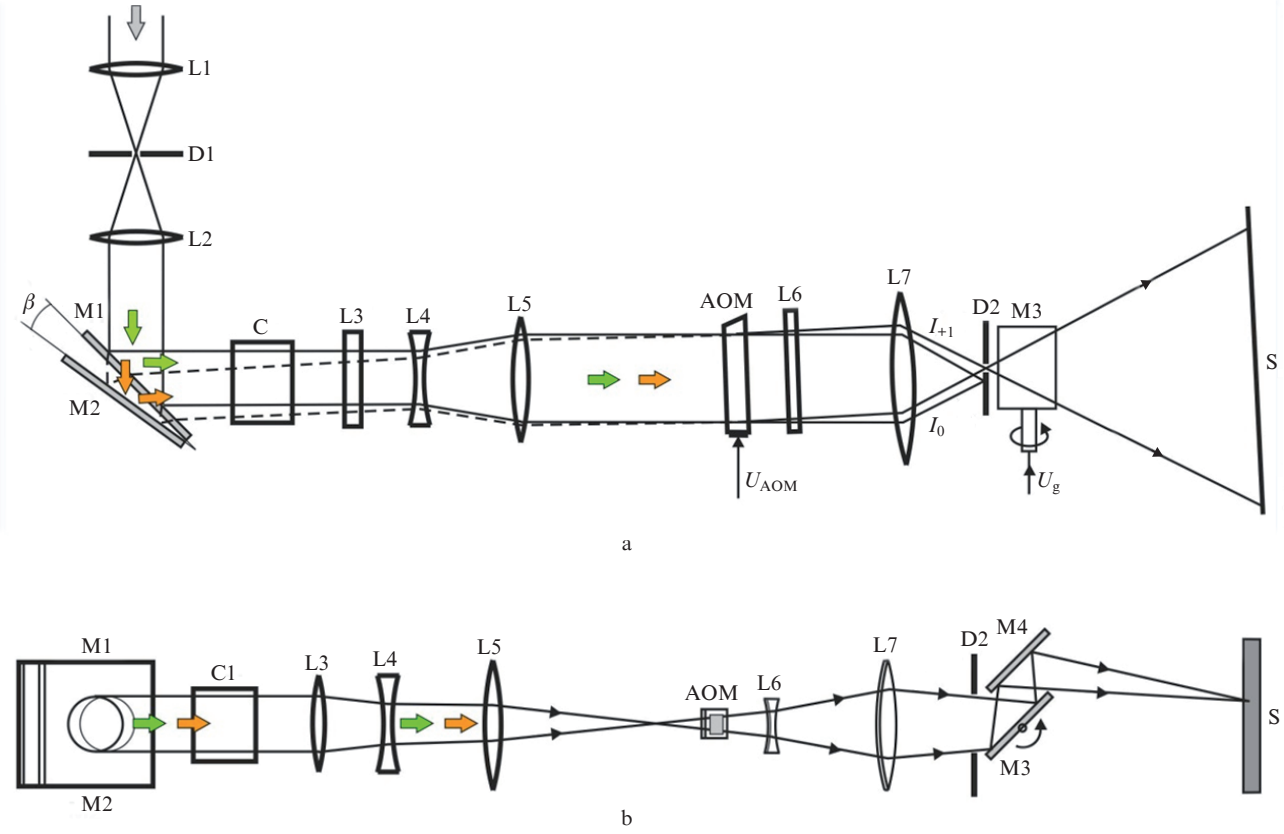

Figure 13. Optical schemes of the television information projection display system in two mutually orthogonal planes (U_{AOM} and U_g are the modulator and galvanometer control signals): (a) horizontal plane coincident with the diffraction plane of the AOM.

laser beams of the two spectral components in the horizontal plane to the dimensions of the working aperture of the AOM and produces convergent beams in the vertical plane. After the beam passes through the aperture converter, the angle between the axes of the beams of the two spectral components with wavelengths λ_1 and λ_2 is $2\beta/M$, where M is the magnification of the matching telescope, consisting of lenses L4 and L5. The two beams impinge on the acousto-optic medium of the AOM at angles θ_{i1} and θ_{i2} in the horizontal plane and then travel through it at angles θ'_{i1} and θ'_{i2}. Mirrors M1 and M2 are located so that the laser beams with wavelengths λ_1 and λ_2 coincide with each other and pass through the aperture of the AOM in the diffraction plane. For the copper vapour laser and one ultrasound carrier frequency f, we can calculate the external angles of incidence $\theta_{i1} = n_o\theta'_{i1}$ and $\theta_{i2} = n_o\theta'_{i2}$ of light beams with wavelengths λ_1 and λ_2 and the angle $\beta = M(\theta_1 - \theta_2)/2$. At $f = 80$ MHz and $M = 1.6$, we obtain $\theta_1 = 0.051$ rad, $\theta_2 = 0.049$ rad and $\beta = 1.6 \times 10^{-3}$ rad.

The AOM output in the first order of diffraction is the spectrum of diffracted light waves, corresponding to the spectrum of the amplitude-modulated acoustic signal. The objective lens L7 visualises the image corresponding to this spectrum on a screen (S). All unnecessary orders of diffraction are eliminated by diaphragm D2. Since the light waves diffract from the same acoustic wave, its visualised images at wavelengths λ_1 and λ_2 should coincide in space. For this purpose, the optical system consisting of lens L6 and objective L7 should be corrected for the absence of chromatic aberration.

As distinct from the optical system in Fig. 6, that in Fig. 13 is built so that the object plane of the image formed on the screen and the light beam focusing plane after the aperture converter are spaced apart from each other. This is due to the fact that the object plane of the anamorphotic corrector consisting of a negative cylindrical lens (L6) and projection objective (L7) coincides with the focal plane of the aperture converter and the object plane of the projection objective coincides with the output aperture of the AOM. As a result, no beam focusing occurs within the AOM crystal. This offers the possibility of operating at high average laser output powers.

In the optical scheme in Fig. 13, the focusing plane of the aperture converter is located in front of the AOM. Placing a cylindrical lens (L6) behind the AOM enables line focusing on the screen in the vertical plane. This is accompanied by optical field averaging on the output aperture of the modulator along the vertical in the image plane, which reduces the influence of structural defects and acoustic field nonuniformities in the modulator on the quality of the line image on the screen.

For vertical scanning, the optical scheme in Fig. 13 employs an electromagnetic mirror galvanometer (M3).

To obviate the third drawback, related to a time delay between light pulses at different wavelengths, a compensator can be placed behind the AOM in order to eliminate the time delay between the television line images for the spectral components with wavelengths λ_1 and λ_2, which will bring into coincidence the light replicas of the television line signal for these components in the object plane of objective L7. Figure 14 shows the optical scheme of a compensator whose operating principle is to separate images according to their colour, transfer the images from the output aperture of the AOM (plane OP1) through two optically identical channels, and then bring the images into coincidence in the intermediate plane OP2, coinciding with the object plane of L7.

For these purposes, the output aperture of the AOM (plane OP1) is placed in front of the beam-splitting mirror M5

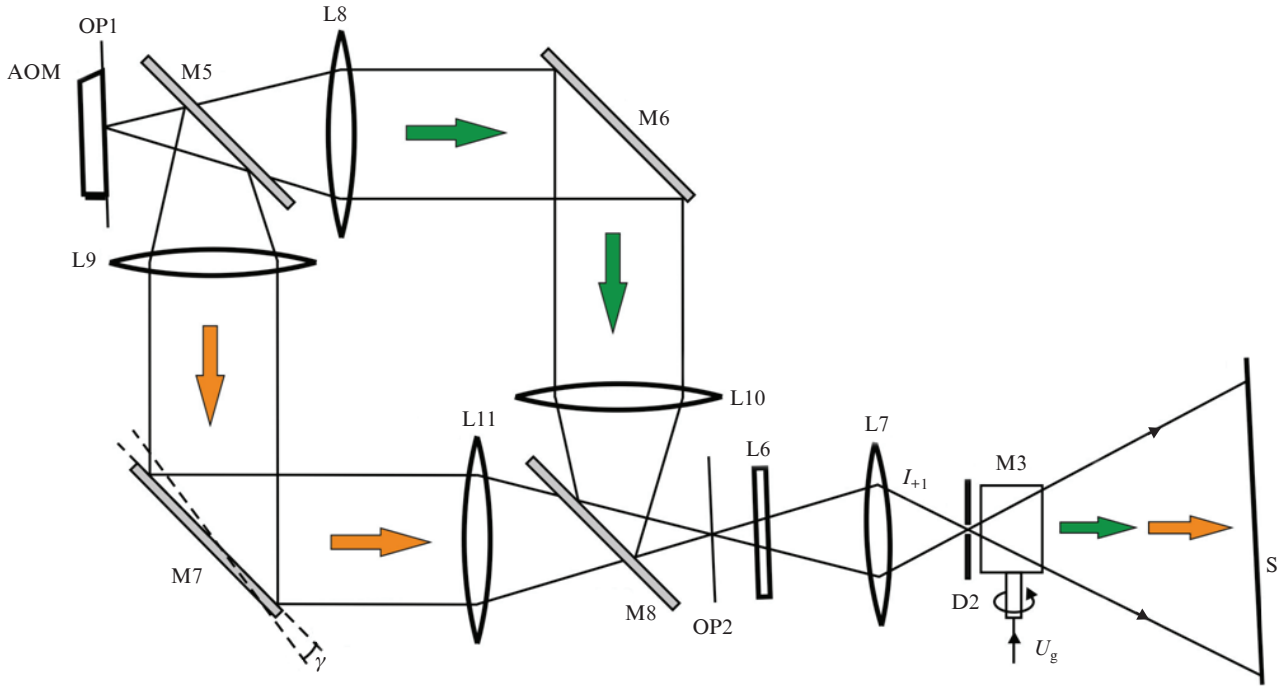

Figure 14. Optical scheme of a compensator of a time delay between images at different wavelengths.

Figure 15. Photographs of television images on the screen of a laser television projector.

so that it coincides with the focal plane of lenses L8 and L9. The laser beam diffracted in the AOM impinges on the dichroic mirror M5 and splits into two spectral components, with wavelengths λ_1 and λ_2. The former spectral component passes through mirror M5 and lens L8. After reflecting from mirror M6, passing through lens L10 and reflecting from mirror M8, it coincides with the latter spectral component in the object plane of the projection objective L7. The latter spectral component of the image travels along its optical path, which includes the same optical components as the optical path of the former component and has the same length. By rotating mirror M7 through a small angle γ, the images at the wavelengths of the two spectral components can be brought into coincidence in plane OP2. Next, the combined image is visualised on a screen by objective L7.

Yet another important feature of the optical system for television imaging with the use of an AOM (Fig. 13) is the large depth of field of the amplitude-modulated signal image, which can be utilised in producing three-dimensional images, for suppressing speckle structures and in the case of screens with uneven surfaces, and allows one to put a screen at a small angle to the imaging system, thereby reducing the transverse dimensions of the television system. The resultant trapezoidal distortions of the raster and the nonlinearity of vertical scanning can be compensated for by electronic means.

Figure 15 shows photographs of a television image on the screen of a laser television projector, which operates under laboratory conditions using a copper vapour laser [47].

9. Conclusions

The acousto-optic laser television display systems considered in this review can find application for controlling the output of high-power pulsed lasers emitting in the visible and IR spectral regions. The existing technology for the fabrication of acousto-optic modulators and deflectors allows one to design and manufacture all-solid-state, easy-to-control, reliable devices operating in real time and capable of withstanding high incident laser powers. The described imaging procedures can find application in special systems, e.g. those that should have no movable mechanical laser beam deflection devices: underwater laser ranging systems for synchronous illumination of objects and high-performance laser systems for layer-by-layer production of complex-shaped three-dimensional structures. They can also be used in mobile information delivery systems for emergency management.

References

1. Korpel A., Adler R., Desmares P., et al. *Proc. IEEE*, **54**, 1429 (1966).
2. Yamamoto M., Taneda T. *Laser Displays, in Advances in Image Pickup and Display.* Ed. by B. Kazan (New York: Academic, 1975; Moscow: Mir, 1979) Vol. 2.
3. Gordon E.I. *Proc. IEEE*, **54**, 1391 (1966).
4. Aksenov E.T., Bukharin N.A., Ignatov A.B., et al. *Tr. Leningr. Politekh. Inst.*, **366**, 69 (1974).
5. Taneda T. et al. *J. SMPTE*, **82** (6), 470 (1973).
6. Gorod J., Knox J.D., Goedertier P.V. *RCA Rev.*, **33**, 623 (1972).
7. Geoffrey G.F. *Radio Electron. Eng.*, **39** (3), 123 (1970).
8. Benedichuk I.V., Oboznenko Yu.L., Smirnov E.I., et al. *Tekh. Kino Telev.*, **6**, 3 (1978).
9. Watson W.N., Korpel A. *Appl. Opt.*, **9**, 1176 (1970).
10. Klima M. *Slaboproudýobzor*, **40**, 415 (1979).
11. Yamada Y., Yamamoto M., Nomura S. *Proc. Conf. 6th Int. Quantum Electron.* (Kyoto, 1970) p. 242.
12. Yamamoto M. *Hitachi Rev.*, **24**, 89 (1975).
13. Nowicki T. *Electro-Opt. Syst. Des.*, **6** (2), 23 (1974).
14. Yamamoto M. US Patent, No. 3818129 (1974).
15. Okolicsanyi F. *Wireless Eng.*, **14**, 527 (1937).
16. Bergmann L. *Ultrasonics* (London: Bell, 1938; Moscow: Inostrannaya Literatura, 1957).
17. Lowry J.B., Welford W.T., Humphries M.R. *Opt. Lasers Technol.*, **20**, 255 (1988).
18. Mokrushin Yu.M., Shakin O.V. RF Patent No. 2 104 617, *Byull. Izobret.*, 28 (1998).
19. Mokrushin Yu.M., Shakin O.V. *J. Russ. Laser Res.*, **17**, 381 (1996).
20. Martinsen R.J., Aylward R.P. *Photonics Spectra*, (11), 109 (1996).
21. Martinsen R.J., Karakawa M., McDowell S.R. *Proc. SPIE Int. Soc. Opt. Eng.*, **3000**, 150 (1996).
22. *Laser Focus World*, **35** (5), 13 (1999).
23. Armstrong J.A., Bloembergen N., Ducuing J., Pershan P.S. *Phys. Rev.*, **127**, 1918 (1962).
24. Franken P.A., Ward H.F. *Rev. Mod. Phys.*, **35**, 23 (1963).
25. Lim E.J., Fejer M.M., Byer R.L. *Electron. Lett.*, **25** (3), 174 (1989).
26. Dmitriev V.G., Tarasov L.V. *Prikladnaya nelineinaya optika* (Applied Nonlinear Optics) (Moscow: Fizmatlit, 2004).

27. Hu X.P. *Opt. Lett*., **33**, 408 (2008).
28. Wallenstein R. US Patent, No. 5.828.424 (1998).
29. Nebel A., Ruffing B., Wallenstein R. *Proc. Laser and Electro-Optics Society Annual Meeting (LEOS IEEE)* (Orlando, Fl, 1998) pp395–396.
30. Nebel A., Ruffing B., Wallenstein R. *Laser Focus World*, **35** (5), 263 (1999).
31. Brunner F., Innerhofer E., Marchese S.V., et al. *Opt. Lett*., **29**, 1921 (2004).
32. Innerhofer E., Brunner F., Marchese S.V., et al. *J. Opt. Soc. Am. B*, **23** (2), 265 (2006).
33. Watson J.P. et al. *Proc. SPIE Int. Soc. Opt. Eng*., **5364**, 116 (2004).
34. Shchegrov A.V. *Proc. SPIE Int. Soc. Opt. Eng.*, **5332**, 151 (2004).
35. Solgaard O., Sandejas F.S.A., Bloom D.M. *Opt. Lett*., **17**, 688 (1992).
36. Bloom D.M. *Proc. SPIE Int. Soc. Opt. Eng.*, **3013**, 165 (1997).
37. Trisnadi J.I., Carlisle C.B., Monteverde R. *Proc. Micromachining and Microfabrication Symp*. (San Jose, CA, 2004).
38. Magdich L.N., Molchanov V.Ya. *Acoustooptic Devices and Their Applications* (New York: Gordon and Breach, 1989; Moscow: Sovetskoe Radio, 1978).
39. Shaskol'skaya M.P. (Ed.) *Akusticheskie kristally* (Acoustic Crystals) (Moscow: Nauka, 1982).
40. Uchida N., Ohmachi Y. *J. Appl. Phys*., **40**, 4692 (1969).
41. Turok I.I., Golovei M.M. *II Vsesoyuzn. konf. Aktual'nye problemy polucheniya i primeneniya segneto- i p'ezoelektricheskikh materialov* (II All-Union Conf. Current Issues in the Preparation and Application of Ferro- and Piezoelectric Materials) (Moscow, 1984) p. 264.
42. Shakin O.V., Kudzin A.Yu., Gorbenko V.M., Akimov S.V., Portretnyi V.P., Grishmanovskii A.N. USSR Inventor's Certificate No. 1 529 785 (1989).
43. Kolesnikov A.I., Kaplunov I.A., Terent'ev I.A. *Kristallografiya*, **49**, 229 (2004).
44. Proklov V.V. *Radiotekh. Elektron*., **25**, 1543 (1980).
45. Goutzoulis A., Pape D., Kulakov S. *Design and Fabrication of Acoustooptic Device* (New York: Marcel Dekker Inc., 1994).
46. Gulyaev Yu.V., Kazaryan M.A., Mokrushin Yu.M., Prokhorow A.M., Shakin O.V. *Laser Phys*., **12** (11), 1368 (2002).
47. Vasil'ev Yu.P., Kazaryan M.A., Mokrushin Yu.M., Prokhorov A.M., Shakin O.V. *Svetotekhnika*, **5**, 7 (1998).
48. Balakshii V.I., Mantsevich S.N. *Akust. Zh*., **58**, 600 (2012).
49. Brillouin L. *Act. Sci. Ind*., **59**, 1 (1933).
50. Raman C.V., Nath N.S.N. *Proc. Ind. Acad. Sci*., **2A**, 406, 413 (1935); **3A**, 75, 119, 459 (1936).
51. Rytov S.M. *Izv. Akad. Nauk SSSR, Ser. Fiz*., **2**, 223 (1937).
52. Quate C.F., Wilkinson C.D.W., Winslow D.K. *Proc. IEEE*, **53**, 1604 (1965).
53. Born M., Wolf E. *Principles of Optics* (Oxford: Pergamon, 1969; Moscow: Nauka, 1970).
54. Soroka V.V. *Akust. Zh*., **19**, 877 (1973).
55. Marcuse D. *Integrated Optics* (New York: IEEE, 1973; Moscow: Mir, 1974).
56. Parygin V.N., Chirkov L.E. *Radiotekh. Elektron*., **18**, 703 (1973).
57. Parygin V.N., Chirkov L.E. *Radiotekh. Elektron*., **19**, 1178 (1974).
58. Parygin V.N., Chirkov L.E. *Kvantovaya Elektron*., **2**, 318 (1975) [*Sov. J. Quantum Electron*., **5**, 180 (1975)].
59. Martynov A.M. *Radiotekh. Elektron*., **22**, 533 (1977).
60. Stashkevich A.A. *Opt. Spektrosk*., **45**, 967 (1978).
61. Balakshii V.I., Parygin V.N., Chirkov L.E. *Fizicheskie osnovy akustooptiki* (Physical Principles of Acousto-Optics) (Moscow: Radio i Svyaz', 1985).
62. Kulak G.V. *Zh. Tekh. Fiz*., **67**, 80 (1997).
63. Kulak G.V., Nikolaenko T.V. *Zh. Prikl. Spektros*k., **73**, 819 (2006).
64. Mikhailovskaya A.S., Mikhailovskaya L.V. *Opt. Spektrosk*., **110**, 317 (2011).
65. Petrun'kin V.Yu., Vodovatov I.A. *Izv. Vyssh. Uchebn. Zaved. Ser. Radiofiz*., **26**, 1570 (1983).
66. Petrun'kin V.Yu., Vodovatov I.A., Vetrov K.V. In: *Obrabotka radiosignalov akustoelektronnymi i akustoopticheskimi ustroistvami* (Radio Signal Processing Using Acousto-Electronic and Acousto-Optic Devices) (Leningrad: Nauka, 1983) p. 51.
67. Petrun'kin V.Yu., Vodovatov I.A., Lipovskii A.A. *Izv. Vyssh. Uchebn. Zaved. Ser. Radiofiz.*, **26**, 1021 (1983).
68. Petrun'kin V.Yu., Vodovatov I.A. *Izv. Vyssh. Uchebn. Zaved. Ser. Radiofiz*., **27**, 332 (1984).
69. Mokrushin Yu.M. *Nauchno-Tekh. Vedom. S.-Peterburg. Gos. Politekh. Univ. Fiz.-Mat. Nauki*, (2), 93 (2011).
70. Mokrushin Yu.M. *Nauchno-Tekh. Vedom. S.-Peterburg. Gos. Politekh. Univ. Fiz.-Mat. Nauki*, (3), 99 (2011).
71. Mokrushin Yu.M. *Nauchno-Tekh. Vedom. S.-Peterburg. Gos. Politekh. Univ. Fiz.-Mat. Nauki*, (4), 118 (2011).
72. Molotok V.V., Razzhivin B.P. *Akustoopt. Metody Tekh. Obrab. Inform*., **142**, 10 (1980).
73. Damon R.W., Maloney W.T., McMahon D.H. In: P*hysical Acoustics*. Ed. by W.P. Mason, R.N. Thurston (New York: Academic, 1970; Moscow: Mir, 1974) Vol. 7.
74. Lemanov V.V., Shakin O.V. *Fiz. Tverd. Tela*, **14**, 229 (1972).
75. Pisarevskii Yu.V., Sil'vestrova I.M. *Kristallografiya*, **19**, 1003 (1973).
76. Uchida N., Ohmachi P. *Jpn. J. Appl. Phys*., **9** (1), 155 (1970).
77. Bogdanov S.V., Bol'sheva T.A. *Avtometriya*, (5), 34 (1985).
78. Petrash G.G. *Usp. Fiz. Nauk*, **105**, 645 (1971).
79. Little C.E. *Metal Vapour Laser: Physics, Engineering and Applicaitions* (Chichester: J. Wiley and Sons, 1999).
80. Lyabin N.A., Chursin A.D., Ugol'nikov S.A., et al. *Kvantovaya Elektron*., **31**, 192 (2001) [*Quantum Electron*., **31**, 192 (2001)].
81. Grigor'yants A.G., Kazaryan M.A., Lyabin N.A. *Lazery na parakh medi: konstruktsiya, kharacteristiki i primeneniya* (Copper Vapour Lasers: Design, Characteristics and Applications) (Moscow: Fizmatlit, 2005).
82. Markova S.V., Petrash G.G., Cherezov V.M. *Kvantovaya Elektron*., **4**, 1154 (1977) [*Sov. J. Quantum Electron*., **7**, 657 (1977)].
83. Linevsky M.J., Karrus T.W. *Appl. Phys. Lett*., **33**, 720 (1978).
84. Zemskov K.I., Isaev A.A., Kazaryan M.A., et al. *Kvantovaya Elektron*., **1**, 863 (1974) [*Sov. J. Quantum Electron*., **4**, 474 (1974)].
85. Belyaev V.P., Zubov V.V., Komal'dinov N.A., et al. *Elektron. Prom–st*., **10** (138), 28 (1984).
86. Du C., Ruan S., Yu Y., Wang Z. *Opt. Express*, **13**, 8591 (2005).
87. Du C., Ruan S., Yu Y., Zeng F. *Opt. Express*, **13**, 2013 (2005).

88. Haiyong Z., Ge Z., Chenghui H., et al. *Opt. Express*, **16**, 2989 (2008).
89. Konno S., Kojima T., Fujikawa S., et al. *Opt. Lett.*, **25**, 105 (2000).
90. Bo Y., Geng A., Bi Y., et al. *Appl. Opt*., **45**, 2499 (2006).
91. Tang H., Xiaolei Z., Junqing M., et al. *Chin. Opt. Lett*., **7**, 812 (2009).
92. Lee D., Moulton P.F. *Proc. CLEO'2001* (Washington, OSA, 2001) paper CThJ2, p. 424.
93. Moulton P.F., Snell K.J., Lee D., et al. *Proc. IMAGE 2002 Conf.* (Scottsdale, Arizona, 2002).